Supplement of The Cryosphere, 14, 4581–4601, 2020
https://doi.org/10.5194/tc-14-4581-2020-supplement

The Cryosphere Open Access EGU

Supplement of

Measurements and modeling of snow albedo at Alerce Glacier, Argentina: effects of volcanic ash, snow grain size, and cloudiness

Julián Gelman Constantin et al.

Correspondence to: Julián Gelman Constantin (juliangelman@cnea.gov.ar)

S1 Methods

We present here additional details of experimental or modeling methodologies.

S1.1 Snow samples. Filters treatment

All samples from snow pits were taken with an aluminum shovel, previously "rinsed" with fresh snow, and preserved in plastic bags (PP or PET). In 2016 campaign we also used a snow/firn hand auger to sample a $2.5\,\mathrm{m}$ snow/firn core (site *Acc2-2016*). The core was sampled in eight different fractions according to the in situ stratigraphy (see Fig. 2 in the manuscript), which were also collected in plastic bags.

All samples were transported to the base camp and stored below melting temperature until processing. Sealed plastic bags were heated in a warm water bath in the mountain hut until complete melting. A fraction of the melted sample was filtered through a Millipore vacuum filter holder (XX1104700), with a plastic hand vacuum pump (XKEM00107). We used polycarbonate filters of $0.4\,\mu\mathrm{m}$ (2016) or $0.8\,\mu\mathrm{m}$ (2017) pore size. The filter material and pore size is thought to be appropriate to collect most of carbonaceous particles without increasing significantly the filtering time (Doherty et al., 2010). Filtered volume was measured after filtering, with a plastic measuring cylinder. All filters were kept in individual plastic boxes. Before field campaigns, unused filters were conditioned in a desiccator for at least 48 hs prior to weighting (Sartorius ME5-F microbalance and Mettler universal anti-static kit). Total PM was determined by weighting (with the same protocol) the $0.4\,\mu\mathrm{m}$ or $0.8\,\mu\mathrm{m}$ filters and subtracting the mass of the unused filters.

S1.2 Albedo corrections

Albedo values were obtained applying Equation S1, which includes corrections related with the diffuse or reflected light blocked by the operator or the mounting stand and, for upwelling radiation, the effect of shadows of the sensor and the stand in the snow surface (Wright et al., 2014; Carmagnola et al., 2013).

$$\alpha = \frac{C_{shadow\uparrow} I_{refl\uparrow}}{C_{shadow\downarrow} I_{diff\downarrow} + I_{dir\downarrow}} \tag{S1}$$

$I_{refl\uparrow}$ is the upwelling reflected radiation, $I_{diff\downarrow}$ is the downwelling diffuse radiation and $I_{dir\downarrow}$ is the downwelling direct radiation. $C_{shadow\uparrow,\downarrow}$ are the correction factors that account for the light obstruction and shadows, and are calculated as follows:

$$C_{shadow\uparrow,\downarrow} = \left(\int_0^{\phi} \int_{\theta}^{\pi/2} \sin\theta \cos\theta d\theta d\phi \right) (1/\pi) \tag{S2}$$

where the integration angles ϕ and θ are represented in Fig. 3 (b) of the manuscript. These equations assume that reflected and diffuse radiation are isotropic. Even though it is known that this assumption is incorrect for the radiation reflected from snow (Dumont et al., 2010), the corresponding error is lower than the uncertainty of the measured albedo (Carmagnola et al., 2013).

To calculate shadows position we needed to calculate the effective incidence angle over the glacier slopes. A simple geometrical relationship was used (Lai et al., 2010):

$$\cos\gamma_{inc} = \cos\theta_{sl}\cos\theta_{zen} + \sin\theta_{sl}\sin\theta_{zen}\cos(\phi_{asp} - \phi_{az}) \tag{S3}$$

where γ_{inc} is the effective angle between the sunbeam and the normal of the sloped surface, θ_{zen} and ϕ_{az} are the zenith and azimuth angles of the sun, θ_{sl} is the average slope of the surface and ϕ_{asp} is the aspect of the slope, measured clockwise from the north.

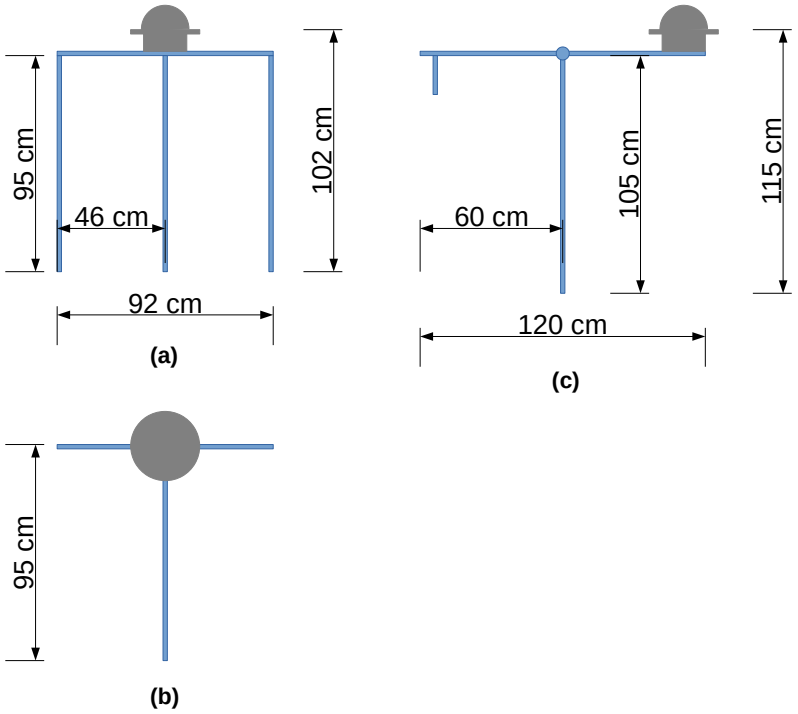

Figure S1. Details of the pyranometer mounting stands in Fig. 3 of the main text. (a) Side view and (b) top view of the mounting stand used in 2016 field campaign. (c) Side view of the mounting stand used in 2017 field campaign.

S2 Dating of snow/firn layers

Most snow/firn layers sampled during both field campaigns were easily dated, considering that the topmost layer contains the most recent snow and attributing layers below based on PM content, density, hardness and grain size. Topmost layers were identified as:

1. fresh snow from a recent deposition events, on the accumulation zone, (sites *Acc1-2016*, *Acc2-2016*, *Acc4-2017*, *Acc5-2017*, *Acc6-2017* and *Acc7-2017*, Fig. S2 (a)), on an accumulation pocket (site *Abl1-2016*), or on top of ablation ice (sites *Abl2-2016* and *Abl5-2017*),
2. end-of-ablation season surface, with high enrichment of PM content (*Acc3-2016*, Fig. S2 (b)), or
3. ablation ice (site *Abl6-2017*).

The only exception were sites *Abl3-2017* and *Abl4-2017*, located in an accumulation pocket in the ablation zone of the glacier. As can be seen in Fig. S2 (c), site *Abl4-2017* corresponded to the topmost layer of the pocket (which disappeared toward the borders of the pocket, site *Abl3-2017*). However, based on the hardness, density, coarse grain size ($(738 \pm 167)\,\mu m$) and high surface enrichment (PM content as high as $(12\,000 \pm 2000)\,mg\,kg^{-1}$), we interpreted that this was a firn layer due to negative net accumulation during 2016-2017 hydrological year. The sub-surface firn layer of site *Abl4-2017*, with a low PM content,

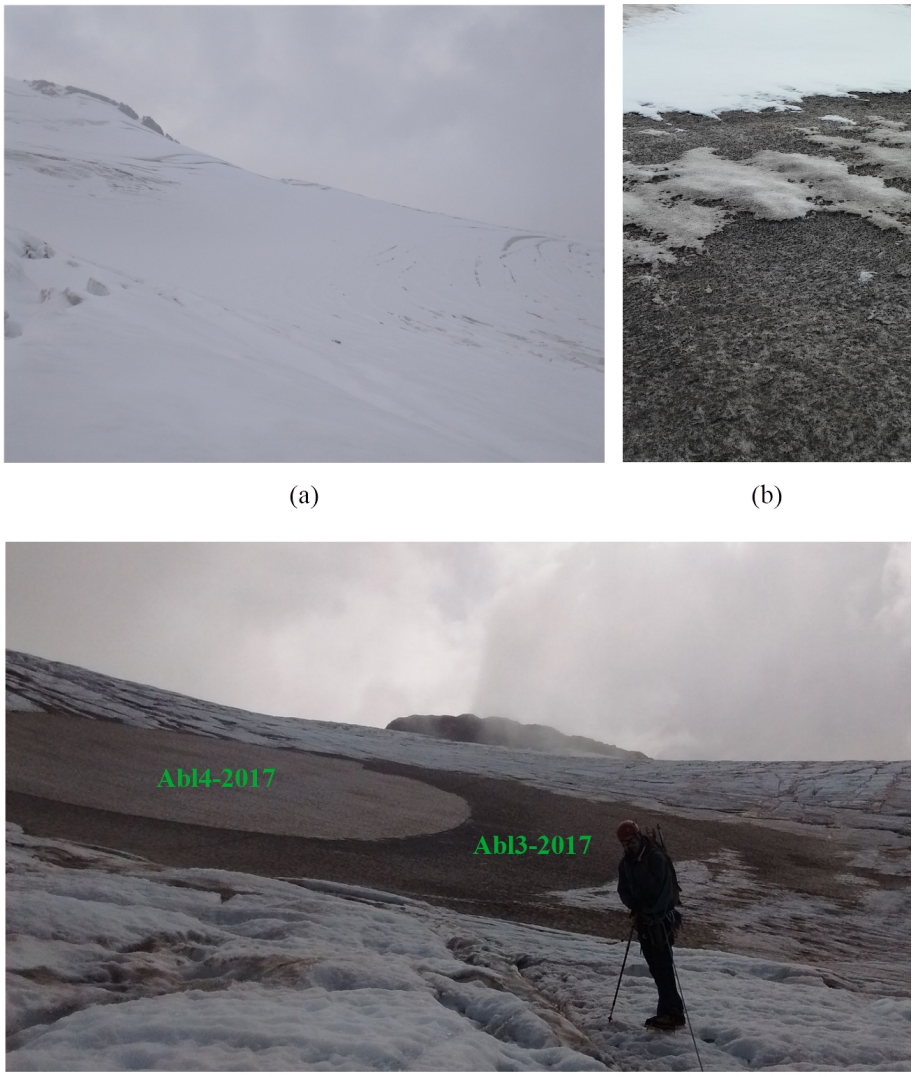

Figure S2. Field pictures of sampling sites. (a) General view of the area of the accumulation zone that includes sites *Acc1-2016*, *Acc2-2016*, *Acc3-2016*, *Acc4-2017*, *Acc5-2017*, *Acc6-2017* and *Acc7-2017* (b) Close view of surface of site *Acc3-2016* (darkest layer, bottom of the picture), next to recent fresh snow (top of the picture). (c) Accumulation pocket in the ablation area of sites *Abl3-2017* and *Abl4-2017*.

was attributed to firn accumulated during 2015 winter. Since those two layers have disappeared in site *Abl3-2017*, this area was identified as an area with even lower specific mass balance, where all accumulation from 2015-2016 hydrological year had also melted. The PM content, $(30\,000 \pm 5000)\,\mathrm{mg\,kg^{-1}}$, is consistent with the expected higher surface enrichment. The sub-surface firn layer was then attributed to accumulation during 2014 winter.

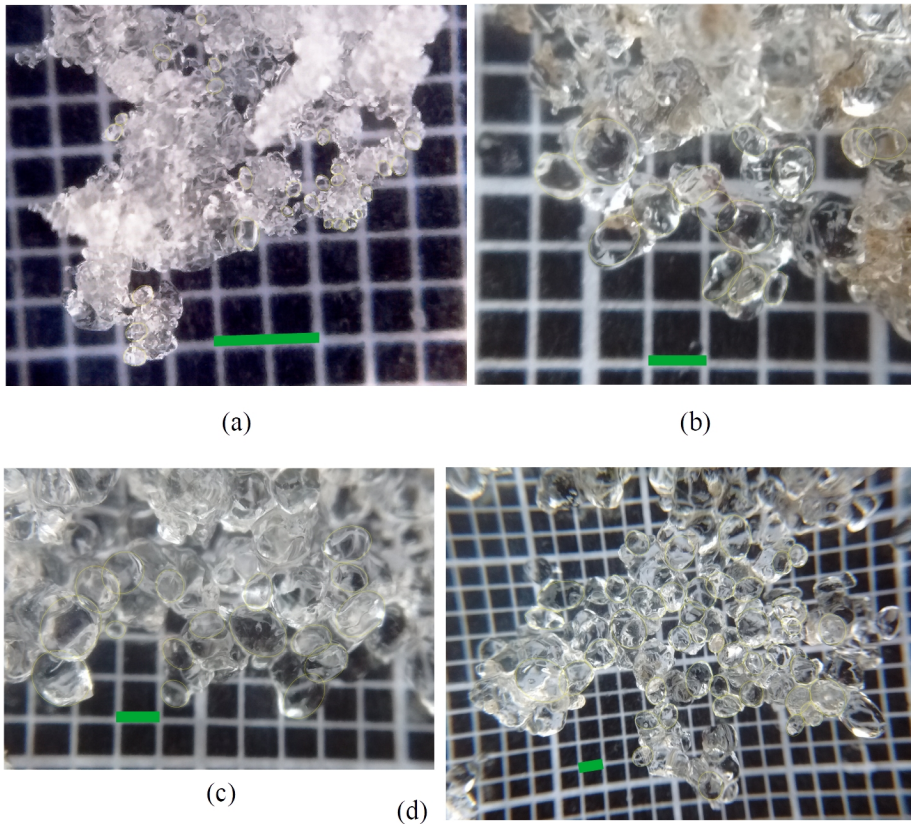

Figure S3. High resolution macro pictures of snow/firn grains, Alerce glacier, 2017. (a) Surface fresh snow sample, April 2017, site *Acc5-2017*. (b) Surface snow/firn sample, attributed approximately to April 2016 (due to negative specific mass balance), site *Abl4-2017*. (c) Sub-surface firn sample, attributed to winter 2015, site *Abl4-2017*. (d) Sub-surface firn sample, attributed to winter 2014, site *Abl3-2017*. In all pictures the green bar width represents $1\,\mathrm{mm}$.

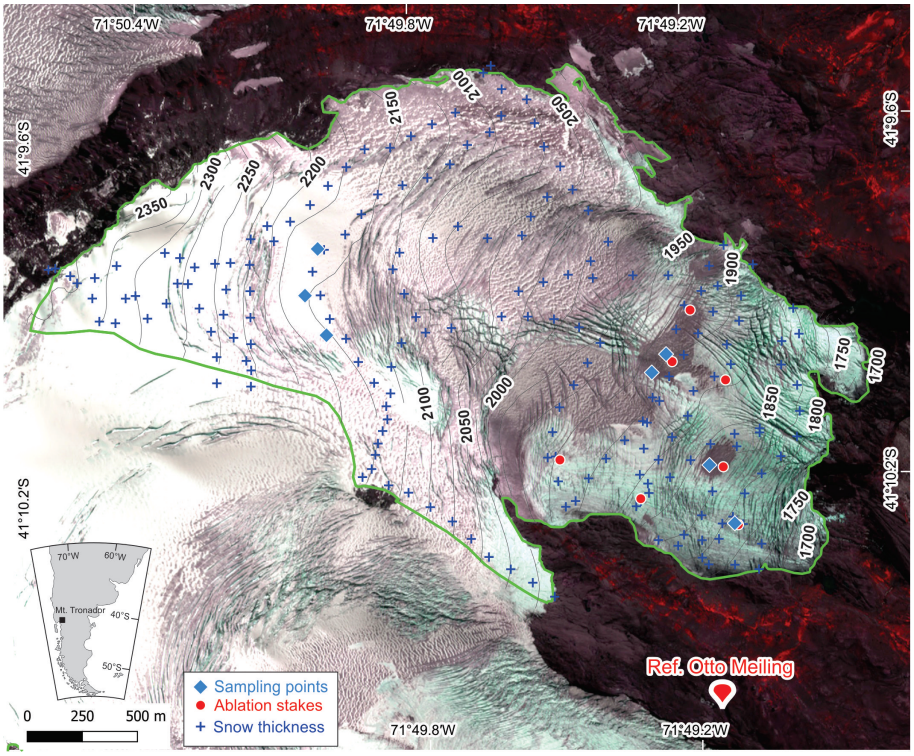

Figure S4. Snow thickness and ablation stakes used for calibration and validation of the mass balance model. Blue rhombuses are albedo and PM sampling points (same as in Fig. 1 of the main article). Background image: false-color pan-sharpened Pléiades satellite image, 7 March 2012, PGO, CNES-Airbus D & S (Ruiz et al., 2015)

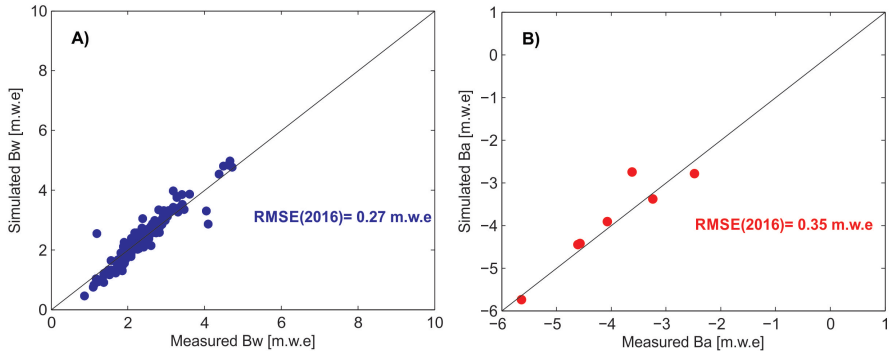

Figure S5. Calibration of the mass balance model with 2016 measurements. (a) First step of the calibration, with winter thickness measurements. (b) Second step of the calibration, with summer specific mass balance measurements (ablation stakes).

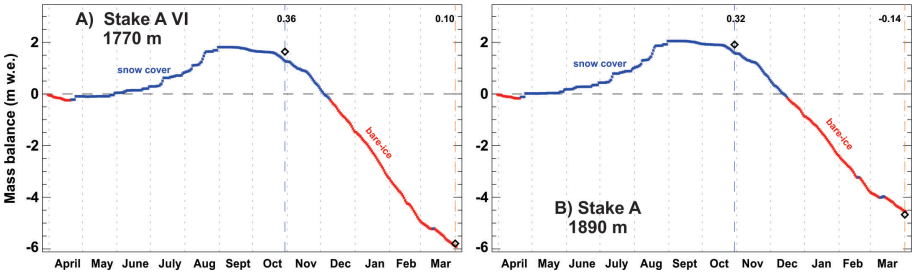

Figure S6. Mass balance model fitting with 2016 measurements for two specific ablation stakes. The residuals between measurements and model it is shown for comparison. Location of (a) stake A VI and (b) stake A are represented in Fig. 1 of the main article.

References

Carmagnola, C. M., Domine, F., Dumont, M., Wright, P., Strellis, B., Bergin, M., Dibb, J., Picard, G., Libois, Q., Arnaud, L., and Morin, S.: Snow spectral albedo at Summit, Greenland: Measurements and numerical simulations based on physical and chemical properties of the snowpack, Cryosphere, 7, 1139–1160, https://doi.org/10.5194/tc-7-1139-2013, 2013.

Doherty, S. J., Warren, S. G., Grenfell, T. C., Clarke, A. D., and Brandt, R. E.: Light-absorbing impurities in Arctic snow, Atmospheric Chemistry and Physics, 10, 11 647–11 680, https://doi.org/10.5194/acp-10-11647-2010, http://www.atmos-chem-phys.net/10/11647/2010/, 2010.

Dumont, M., Brissaud, O., Picard, G., Schmitt, B., Gallet, J. C., and Arnaud, Y.: High-accuracy measurements of snow Bidirectional Reflectance Distribution Function at visible and NIR wavelengths - comparison with modelling results, Atmospheric Chemistry and Physics, https://doi.org/10.5194/acp-10-2507-2010, 2010.

Lai, Y.-J., Chou, M.-D., and Lin, P.-H.: Parameterization of topographic effect on surface solar radiation, Journal of Geophysical Research, 115, D01 104, https://doi.org/10.1029/2009JD012305, http://doi.wiley.com/10.1029/2009JD012305, 2010.

Ruiz, L., Berthier, E., Masiokas, M., Pitte, P., and Villalba, R.: First surface velocity maps for glaciers of Monte Tronador, North Patagonian Andes, derived from sequential Pléiades satellite images, Journal of Glaciology, 61, 908–922, https://doi.org/10.3189/2015JoG14J134, 2015.

Wright, P., Bergin, M., Dibb, J., Lefer, B., Domine, F., Carman, T., Carmagnola, C., Dumont, M., Courville, Z., Schaaf, C., and Wang, Z.: Comparing MODIS daily snow albedo to spectral albedo field measurements in Central Greenland, Remote Sensing of Environment, 140, 118–129, https://doi.org/10.1016/j.rse.2013.08.044, http://dx.doi.org/10.1016/j.rse.2013.08.044, 2014.